जलवायु
JALAWAAYU
(Interdisciplinary Journal of Atmospheric and Hydrospheric Sciences)
Journal home page: https://cdhmtu.edu.np/journal/index.php/jalawaayu

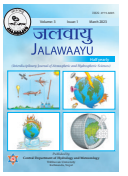

Type of paper: Original Article

A Meteorological Analysis from the Southern Slope of Mt. Everest, Nepal

Kaman Ghimire[1], Arnab Singh[1], Arbindra Khadka[2], Dibas Shrestha[1,*], Binod Dawadi[1,3]

[1] Central Department of Hydrology & Meteorology, Tribhuvan University, 44613, Kathmandu, Nepal
[2] Institute of Research Department, Grenoble, France
[3] Kathmandu Center for Research and Education, Chinese Academy of Sciences – Tribhuvan University, 44613, Kathmandu, Nepal

ARTICLE INFO

Received: 11 December 2022
Received in Revised form: 6 January 2023
Accepted: 31 January 2023
Available Online: 12 February 2023

Keywords

High Altitude Meteorology
Precipitation
Glacier
Mt. Everest

**Correspondence*
Dibas Shrestha
E-mail: dibas.shrestha@cdhm.tu.edu.np

Abstract : Mt. Everest is the highest mountain in the world, with an elevation ending at 8848.86 m above sea level, providing unique opportunity for direct observation of the upper troposphere. Utilizing the data from recently established five automatic weather stations (AWSs) network along the Everest climbing route, as part of the National Geographic and Rolex Perpetual Planet Expedition to Mount Everest 2019, from June 2019 to May 2020, this study investigates the meteorological environment over the southern slope of the Mt. Everest. Precipitation, temperature, radiations (income and outgoing short wave and long wave radiation), wind speed and direction along with derived variables like Lapse Rate, Precipitation Gradient, 6.11 hPa Isoline, and zero-degree Isotherm are analyzed with the aim of understanding altitudinal variation. Precipitation is mainly concentrated in monsoon with highest in Phortse (530 mm). Analysis of temperature lapse rate shows the highest lapse rate (-5.6℃ km^{-1}) in monsoon and lowest in post-monsoon (-7℃ km^{-1}). The precipitation analysis reveals that the vertical

Cite this paper: Ghimire, K., Singh, A., Khadka, A. .,Shrestha, D. & Dawadi, B. A Meteorological Analysis from the Southern Slope of Mt. Everest, Nepal. *Jalawaayu*, *3*(1), 73–96. https://doi.org/10.3126/jalawaayu.v3i1.52069

and horizontal precipitation gradient for monsoon is -63 mm km^{-1} and is -8.6 mm km^{-1} however, during the post-monsoon, precipitation increased by 0.75mm km^{-1} and 4.6 mm km^{-1}, respectively. Similarly, westerly winds dominate during winter in upper station while it's nearly uniform for lower stations. Radiation, likewise, are highly correlated between the stations, with incoming shortwave being the highest in the upper station, South-Col. Both isoline and isotherm lines are observed at around 6000 m above sea level. The one-year data has revealed some of the interesting pictures of high-altitude meteorology, but long-term data with fewer data gaps should be required to confirm these patterns.

1. Introduction

Mountains are important perturbation factors to large-scale atmospheric flows. They also have an influence on the formation of clouds and precipitation in their vicinity, which is, in turn, indirect mechanisms for vertical exchange of heat and moisture (Ouyang et al., 2020; Perry et al., 2020; Yang et al., 2018). In addition, snow and ice, stored in the mountainous region, are the main source of fresh water for millions of people living downstream. But, the mountains are warming rapidly in the recent decades—accelerating mountain cryosphere shrinkage at an alarming rate worldwide. However, there are no sufficient studies done concerning meteorological conditions on glaciered catchments and the glacier-climate interactions. The paucity of such studies is because of the rough topography and extreme weather conditions.

The high altitude of the southern slope of Mt. Everest in Nepal induces a greater variation in meteorological conditions in space and time. Precipitation regime, dominated by the summer monsoon, shows sharp south-north contrast (Cannon et al., 2017; Sherpa et al., 2017; Shrestha et al., 2012), with rain falling in much of the lower elevation and snow in the higher elevation (Immerzeel et al., 2014; Yang et al., 2018). Surface temperature also shows variation based on the monsoon cycle, with temperatures decreasing below -20 ℃ in winter and rising in subsequent months (Salerno et al., 2015). These underlying interaction between the terrain and meteorological conditions affects the cryospheric processes, including the melt processes (Khadka et al., 2022; Pratap et al., 2019; Shea et al., 2015).

Climate change is predicted to affect cryosphere processes, with rapid glacier shrinkage (Wagnon et al., 2021), snow and ice runoff increasing up to 2050 and thereby decreasing (Khadka et al., 2014; Rees & Collins, 2006). With glaciers sensitive to such climate change, and the country's economy tied to water resources, detailed, high-resolution remote sensing data from the region could be a source but needs ground validation (Immerzeel et al., 2010; Khadka et al., 2022; Wagnon et al., 2021). There is a lack of availability of sufficient hydrological and meteorological data of the high-altitude (>4000m) regions of the Nepal Himalaya (Khadka et al., 2022; Matthews et al., 2022; Shea et al., 2015). In addition, the complex orography results in major climatic variability over short horizontal distances, and the representativeness of limited measurements need to be addressed (Maussion et al., 2014).

A detailed meteorological dataset is needed, not just for understanding climate-glacier feedback, but also for remote sensing and model validation. Thus, five meteorological stations established by National Geographic Society and Rolex Perpetual

Planet Expedition around Everest expedition route, up to 8400 meter, presents us with unique opportunity to not just update and extend previous studies (Mathews et al. 2020, Shea et al., 2015) but also to validate the models (Dawadi et al., 2021) and understand the critical role driven by meteorology for glacial evolution. Several studies has been conducted using Everest station(Grey et al., 2022; Khadka et al., 2021; Matthews et al., 2020; Matthews et al., 2022; Perry et al., 2020; Perry et al., 2021) , however detail analysis of meteorological variables covering all season of the year and its diurnal cycle has not been done yet. Thus, this study aims to presents a detail meteorological analysis using some of the world's highest AWSs.

2. Material and method

2.1 Study Area

The study area lies the northern part of the well-known Khumbu valley, located in the boundary region between Nepal and Tibet Autonomous Region of China (Figure 1). The valley is one of the heavily glacierized area in Nepal with elevation ranging from 3810 to the top of the world Mt. Everest 8448 m above sea level (a. s. l.). This is one of the most popular travel destinations in the world, which attracts 10s of thousands of trekkers and climbers every year.

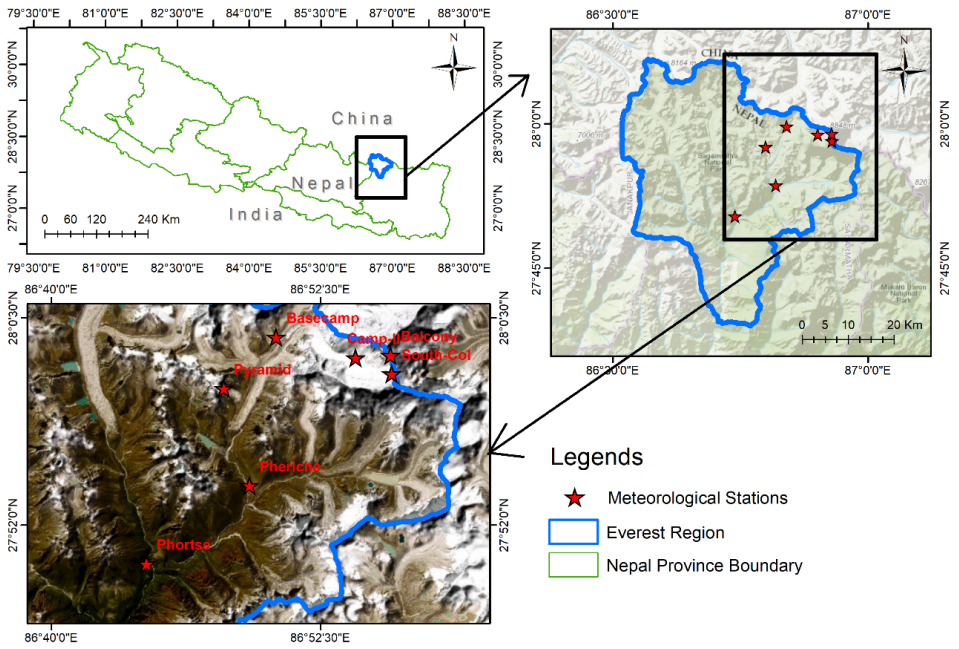

Figure 1. *Study area and locations of the automatic weather station at Mt. Everest region.*

2.2 Data

In this study, five new automatic weather stations established along the southern slope of Mt. Everest in April and May 2019 by the National Geographic and Rolex's Perpetual Planet Everest Expedition were used (Matthews et al., 2020; Perry et al., 2020). In addition, AWSs operated by Institute of Research for Development France (IRD) and Central Department of Hydrology and Meteorology Tribhuvan University (CDHM) at Pyramid (5035 m a. s. l.) and Pheriche (4260 m a. s. l.) were also used. The lower most Phortse AWS (3810 m a. s. l.) is installed in the flat grassy land surface. Basecamp AWS (5315 m. a. s. l.) is in the vegetated medial moraine, just opposite side of the Khumbu Ice Fall. Camp-II AWS (6464 m a. s. l) is in the valley between the two ridges Everest -Nuptse on Khumbu glacier. South-Col AWS (7945 m a. s. l.) is in the flat rock and Balcony AWS (8430 m a. s. l.) was the highest AWS station of the world when it was installed, lies on the ridge of Mount Everest (Matthews et al., 2020). AWS at Pheriche (4260 m a. s. l.), and Pyramid (5035 m a. s. l.) are in the glaciated valley and grassy old moraine, respectively. Details of the installed sensors, measured parameters, and recorded data period are shown in Table 1.

Table 1. *Station location, elevation, observation, sensor, data period and data gap (T = Temperature, RH = Relative Humidity, U = Wind speed, Θ = Wind direction, InSw & OutSw = Incoming & outgoing shortwave radiation, InLw & OutLw = Incoming & outgoing longwave radiation, P = precipitation, BP= Barometric pressure).*

Site	Elevation	Observation	Sensor	Data Period	Data gap
Phortse	3810 m	T, RH, Θ, U P, InSw, OutSw, InLw, OutLw, BP	VaisalaHMP 155A-L5-PT, Young 05108-45, OTT Pluvio2 1500, Hukseflux SR30, Hukseflux IR20, Vaisala PTB110	2019/06/01 to 2020/05/31	
Pheriche	4400 m	P	Geonor T-200B	2019/06/01 to 2019/10/01	
Pyramid	5035 m	T, RH, Θ, U, InSw, OutSw, InLw, OutLw, P	Young 05103-5, Young 05108-45, Kipp& Zonen CNR4 Geonor T-200B	2019/5/30 to 2020/04/17	

Basecamp	5364 m	T, RH, P, BP	VaisalaHMP 155A-L5-PT, OTT Pluvio2 1500, Vaisala PTB110	2019/10/11 to 2020/06/07	From 2019/05/05 to 2019/10/10 (all data were removed due to irregular period) Only temperature, precipitation, and relative humidity data are used
Camp-II	6464m	T, RH, U, Θ, InSw, OutSw, InLw, OutLw, BP	VaisalaHMP 155A-L5-PT, Young 05108-45, Apogee SN-500-SS, Vaisala PTB210	2019/06/11 to 2020/06/07	
South-Col	7945 m	T, RH, U, Θ, InSw, OutSw, InLw, OutLw, BP	VaisalaHMP 155A- L5-PT, Young 05108-45, Hukseflux NR01, Vaisala PTB210	2019/05/22 to 2020/05/27	
Balcony	8430 m	T, RH, U, Θ, BP	VaisalaHMP 155A-L5-PT, Young 05108-45, Vaisala PTB210	2019/06/01to 2020/01/20	After 2020/01/20 station does not work

3. Methodology

3.1 Identification of Errors

The data downloaded from the AWSs needs to filter, sometimes corrected before the analysis due to the unusual dataset. For example, the temperature in Camp-II was showing positive in post-monsoon when there are not positive temperature in Base-Camp. Similarly in the same location, at 2 pm, the temperature was -10oC but one hour later it was 5oC. These types of data were removed from analysis. Only Phortse had a complete precipitation record. Basecamp's precipitation data logger was repaired in September, 2019. For the seven AWSs, the values of incoming shortwave radiation (InSw) lower than 7 w m-2 were set to zero. When the incoming shortwave data is less than 7 w m-2 and outgoing shortwave is less than 6 w m-2, the data were replaced by 0. The maximum albedo was corrected to 0.95 for the observations where albedo exceeds 0.95. When the albedo value is found above 0.95 as in Shea et al., (2015), the shortwave incoming is recalculated by

$$\mathrm{InSw} = \frac{\mathrm{SwOut}}{0.95} \quad (1)$$

3.2 Derived Meteorological Variables

3.2.1 Actual Vapor pressure

For analysis we converted each meteorological variables like temperature, windspeed, precipitation, incoming long-wave and short-wave radiation to daily mean from hourly data. We also divided year into four seasons: monsoon (June-September), post-monsoon (October-November), winter(December-February) and pre-monsoon(March-May). For diurnal cycle we calculated standard deviation of each variable in every station to represent the spread about the mean. For actual vapor pressure, we took an account of saturation vapor pressure and relative humidity from 0 to 100%, which is given below.

$$e_a = e_s \times RH \tag{2}$$

$$e_s = 6.12 \times e^{\frac{17.67 \times T}{243.5+T}} \tag{3}$$

Where T is the observed temperature in ℃.

3.1.2 Vapor pressure, Temperature and Precipitation Gradient

Vapor pressure gradient (Ye_a, hPa km-1) and temperature gradient (Y_t, ℃ km-1) were calculated, which provided important information for distributed melt models, as follows.

$$Ye_a = \frac{e_{a_1} - e_{a_2}}{Z_1 - Z_2} \tag{4}$$

$$Y_t = \frac{T_1 - T_2}{Z_1 - Z_2} \tag{5}$$

Where, Z_1 and Z_2 are elevation of automatic weather stations having actual vapor pressure e_(a_1) & e_(a_2)and temperature T_1 & T_2 respectively.

All precipitation data were converted into both hourly and daily. Precipitation gradients were analyzed as a function of elevation, distance along the valley, latitude, and longitude both annually and seasonally. Here, we calculated the vertical precipitation gradient (mm/m) is defined as,

$$PG = \frac{P_1 - P_2}{Z_1 - Z_2} \tag{6}$$

Where, P_1 and P_2 are the precipitation sums of the highest and lowest points (in mm) and Z_1 and Z_2 are their respective elevations.

3.1.3 Zero-degree Isotherm and 6.11 hPa Isoline

The calculation of latent heat flux and sensible heat flux requires for energy balance model to estimate the near-surface temperature and vapor pressure. The zero-degree isotherm and 6.11hPa isoline elevation helps in understanding of the seasonal change in equilibrium line elevation. The 6.11hPa isoline also controls the energy gain and loss at the surface (Shea et al., 2015). Zero-degree isotherm and 6.11hPa isoline, gives important information about the precipitation phase and the melting condition on glacier surface. The zero-degree isotherm and 6.11 hPa isoline is calculated from the temperature gradient and vapor pressure gradient as follows,

$$Z_{T=0} = \frac{-T_a}{Y_a} + Z_a \quad (7)$$

$$Z_{ea=6.11} = \frac{6.11 - e_a}{Ye_a} + Z_a \quad (8)$$

Where, T_a, e_a and Z_a are temperature (T, °C), actual vapor pressure (e_a, hPa), and elevation of AWS.

Albedo was calculated by using the formula (Fujita & Sakai, 2000)

$$á = \frac{OutSw}{InSw} \quad (9)$$

Where InSw and OutSw are incoming and outgoing shortwave radiation.

4. Results and Discussion

4.1 Comparison of Daily Meteorological Components

Continuous study of meteorological variables is important to understand the overall meteorological condition and changing pattern. This study presents a detail analysis of temperature trend, form and pattern of precipitation, temperature gradient, vapor pressure gradient, zero-degree isotherm, and 6.11hPa isoline at different time scale

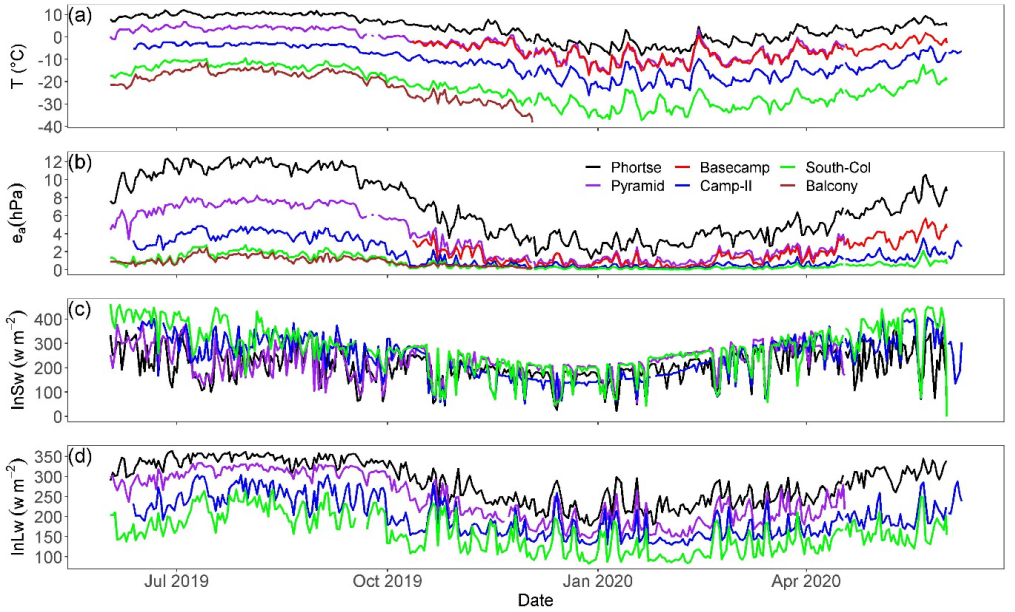

Figure 2. *Summary of 2019-2020 mean daily (a) air temperature (T ℃), (b) actual vapor pressure (ea, hPa), (c) incoming shortwave (InSw, w m-2) and (d) incoming longwave (InLw, w m-2) radiation.*

4.1.1 Air Temperature

The mean daily temperature, aggregated from hourly data from six AWS shows the higher stations have weaker seasonal variations of air temperature than the lower stations (Figure 2). In monsoon, temperature shows less variability and is high during winter. The mean daily temperature are highly correlated between the stations (r=0.70-0.98), especially between Camp-II and South-Col (r=0.98) and less between Phortse and Balcony (r=0.70).

Temperature shows the strong diurnal cycle of daytime heating at Phortse, Pyramid and Basecamp stations whereas higher stations shows weak pattern (Figure 3). The minimum temperature at Balcony station is during the early morning, at around 6-7 A.M., while the maximum temperature is observed during the afternoon (1-2 P.M.). At South-Col, the maximum temperature reaches at 3:00 P.M. Despite having a small difference in distance and elevation between Pyramid and Base camp. These station shows different temperature characteristics during post-monsoon, winter, and pre-monsoon. The pyramid shows early heating than the Basecamp which may be due to the (i) location of the station i.e., Basecamp station lies on the slop facing towards the south east and Pyramid in the valley and (ii) valley wind circulation and daytime radiation between the two stations (Khadka et al., 2019; Shea et al., 2015).

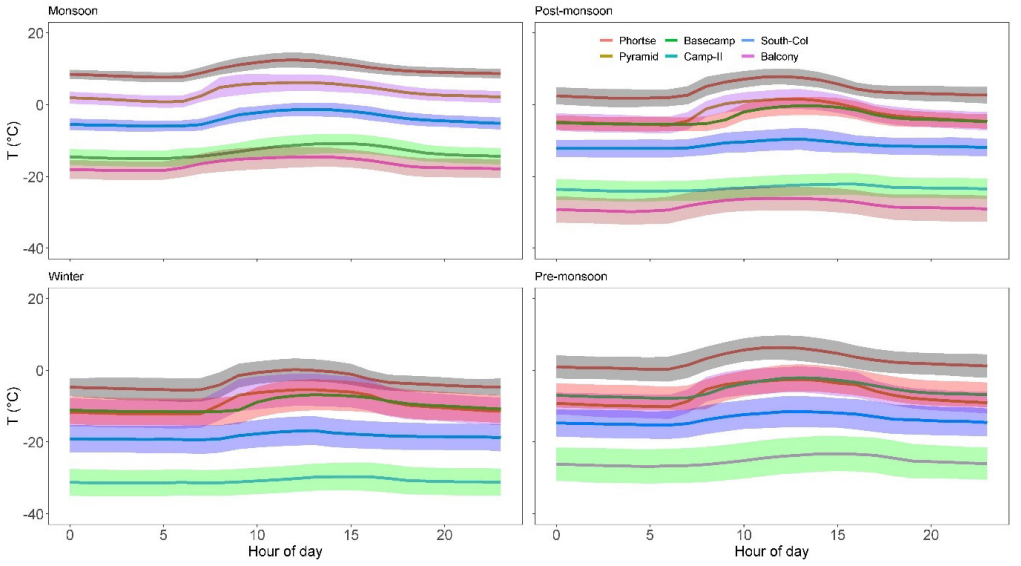

Figure 3. *Diurnal cycle of temperature for Monsoon, Post-monsoon, Winter, and Pre-monsoon. Solid lines show the hourly mean and the shaded portion gives the plus-minus of standard deviation.*

4.1.2 Vapor Pressure

The evolution of the actual vapor pressure calculated from relative humidity and air temperature show high correlation (r=0.77-0.98) in the daily time step. Most of the mean daily value of vapor pressure calculated at Phortse AWS is higher than other AWS sites (Fig. 2), indicating the presence of a high amount of moisture in the lower stations and systemic decrease as the elevation increase. At seasonal scale, vapor pressure is found lowest in winter and gradual increase after pre-monsoon at all stations. Seasonal variation of vapor pressure is found less pronounced in two higher stations, South-Col and Balcony, where value reached up to 3hPa. While, during the winter season, vapor pressure is found less than 1hPa at these stations (Figure 2).

The diurnal pattern of vapor pressure also shows high variation with higher value during 3:00 to 4:00 P.M and minimum during 7:00 to 8:00 A.M. According to season, the value is found minimum in winter and maximum in the monsoon (Figure 4). In pre-monsoon and post-monsoon, the diurnal cycle of vapor pressure is more gradual than the observed temperature. Above the Camp-II station, the vapor pressure remains <2 hPa in all seasons. Overall seasonal and diurnal pattern of vapor pressure is observed as similar as reported by Khadka et al., (2019).

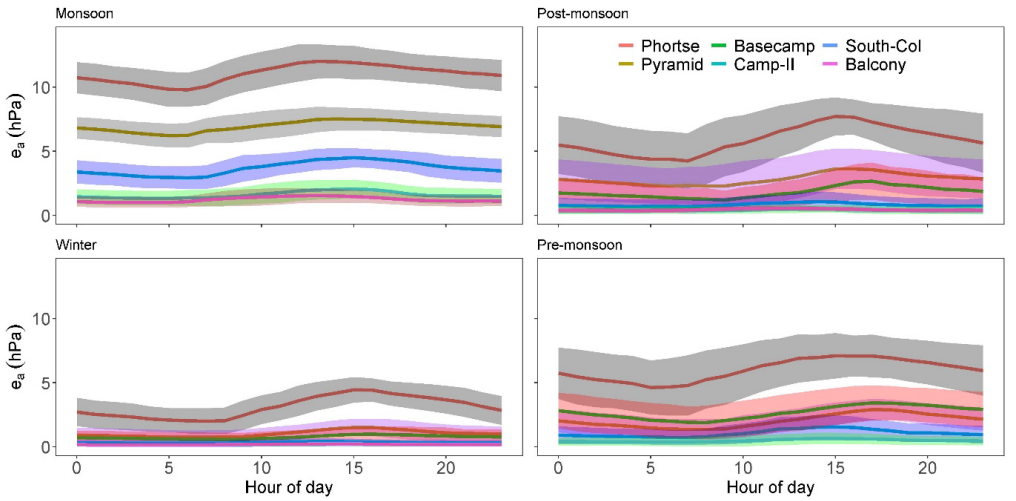

Figure 4. *Diurnal cycle of actual vapor pressure for Monsoon, Post-monsoon, Winter, and Pre-monsoon at different AWS sites. Solid lines show the hourly mean and the shaded portion gives the plus-minus of standard deviation.*

4.1.3 Incoming shortwave and longwave radiation

At all stations, incoming shortwave radiation increases from winter to pre-monsoon and after the monsoon onset, incoming radiation starts to decrease due to the increase in cloudiness (Figure. 2c). In contrast, the incoming longwave radiation shows the opposite pattern, higher in monsoon and lower in winter (Figure. 2d). At higher altitude stations incoming long-wave radiation is low than the lower altitude station (Figure. 2c). The correlation coefficient of mean daily incoming shortwave radiation is moderate (r=0.66-0.88). The highest correlation is found at Camp-II and South-Col (r=0.88). The incoming shortwave is less during the pre-monsoon and monsoon season. At the lower station it is mainly associated with the moist condition and frequently high cloud presence whereas at the high elevation station i.e. South-col station has higher incoming shortwave radiation due to lower air mass, water vapor content, aerosol concentration (Yang et al., 2010), and maximum reflection from the nearby snow-cover surface (Perry et al., 2021).

The incoming longwave radiations are low during winter at all stations and higher during monsoon. There is a steep decrease in incoming longwave after monsoon, indicating withdrawal of monsoon from the Everest region. The data show that the downward longwave radiation decreases as an elevation increase (Figure 2d) due to the higher stations having weaker seasonal variations of air temperature than the lower stations. The cause of such variation is due to the seasonal variation of air temperature; relative humidity and cloud cover (Yang et al., 2018). The correlation between these four stations stands 0.77 to 0.95 and the highest correlation between Camp-II and South-Col station (r=0.95).

The diurnal cycle of mean downwelling longwave follows the same pattern as temperature and vapor pressure (Figure 3, 4 and 5). Maximum values are found during the late afternoon, and minimum values are observed between 7:00 to 8:00 A.M. in all season (Figure 5.). These incoming long waves are highly affected by the cloud cover and the wind pattern in the area. High fluctuation of the incoming longwave at Camp-II during all seasons is due to its unique location and cloud movement over the region. Besides, emission from the steep and high mountain slope (Nuptse north face and Everest south face) could be the important factor. The afternoon peak over the higher elevations station implies more clouds in the daytime could considerably weaken solar radiation(Yang et al., 2010). In monsoon, during daytime, there is an increase in incoming longwave radiation. This decreases in post-monsoon, winter, and pre-monsoon.

As solar radiation is the major energy to drive snow and glacier melting, it is very important to understand its abnormal pattern (higher elevation receives less solar radiation) in this region (Yang et al., 2018). The observed incoming shortwave radiation is high in South-Col station but incoming longwave is low compared to other stations. This indicates the relatively low cloud cover at the elevation and higher exposure of the higher stations.

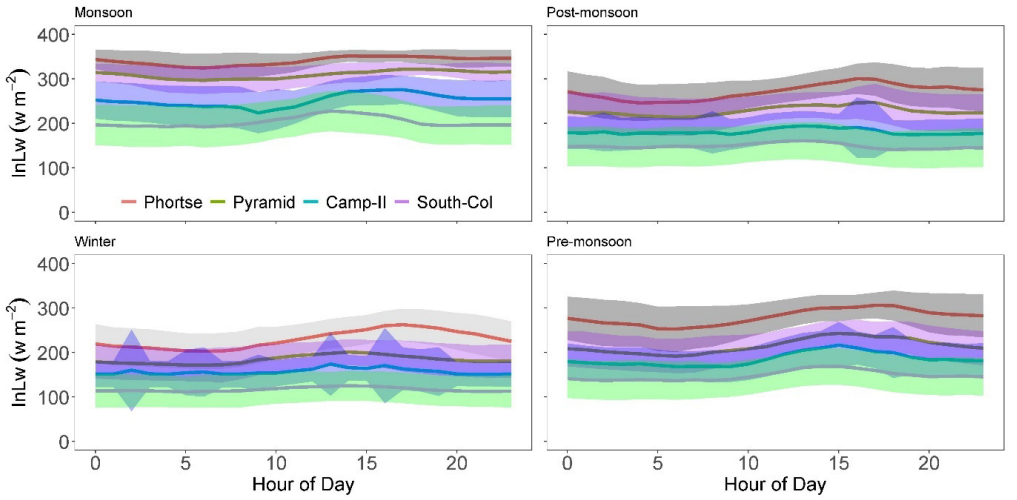

Figure 5. *Diurnal cycle of downwelling longwave for Monsoon, Post-monsoon, Winter, and Pre-monsoon at different AWS sites. Solid lines show the hourly mean and the shaded portion gives the plus-minus of standard deviation.*

4.1.4 Wind Speed and Direction

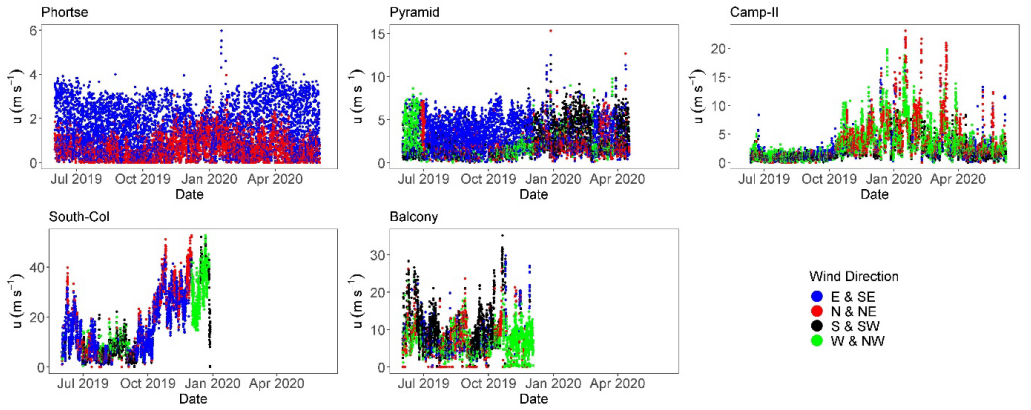

Figure 6. *The wind speed in different direction in different AWS. Where, blue, red, black, and yellow represent the East & South-Easterly, North & North-Easterly, South & South-Westerly, and Westerly & North-Westerly.*

A uniform wind speed is observed over lower stations (Figure 6: Phortse and Pyramid), though the direction is variable. This is not so in higher stations, with winter having highest wind speed in all three stations (Figure 6: Camp-II, South-Col, and Balcony). West and Northwesterly winds dominate in winter. The highest wind speed is found at the South-Col station in winter (45.91 m s-1). Anemometer stopped working after that. On the Balcony highest wind speed (29.20 m s-1) is recorded in post-monsoon. Compared to Balcony station, South-Col has the highest wind speed because the Balcony AWS is located in a more sheltered location (Matthews et al., 2020). At both South-Col and Balcony stations, the up-valley wind is strong and mainly affected by the strong north-westerly wind during winter. At Camp-II station, mean daily wind speed is found greater than 3 m s-1 with the highest value greater than 17 m s-1 during the winter season. At the lower station, Phortse and Pyramid, the mean daily wind speed is found between 1-3 m s-1.

In Phortse AWS there is a clear distinction of the direction of winds. In monsoon, easterly and southeasterly winds dominate while in winter, it is the north and north-easterly winds that gain prominence, though the wind speed barely exceeds 3 m s-1. The highest wind speed is observed during April blowing from east and southeast. It is important to note that there is an absence of westerly wind at Phortse throughout the year which might have been due to the mountains in the western side that blocks the westerly winds.

In Pyramid AWS, the monsoon and winter distinctions are not clear. westerly and northwesterly winds dominate in early June and July and as the monsoon has settled, it is easterly winds that come to dominate and well into post-monsoon. The beginning of winter sees westerly dominance, particularly from the south well into the early pre-monsoon. The maximum wind speed is also reached during this period.

The distinction becomes even more muddled in Camp-II AWS, with no clear wind direction found during pre-monsoon, monsoon, and post-monsoon. The bell-shaped curve is quite interesting with wind speed increasingly rapidly with the onset

of November and decreasing with the onset of March. It is the northerly winds that dominate in winter and wind speed reaches its peak.

Unlike the bell-shaped curve of Camp-II AWS, the South-Col AWS has periodic rise and fall of wind speed. However, due to the loss of data at the beginning of 2020 due to the strong gust, we cannot fully surmise if the same pattern is also in pre-monsoon. Easterly and southeasterly winds dominate well into December, however, the strong gust in November is due to north and north easterly wind. The abrupt end to easterly wind gives way to westerly winds during mid-December, highlighting the influence of westerly jet from that time onwards.

In the higher Balcony station, there is no influence of easterly winds. Perhaps the monsoon circulation doesn't reach the height of the Balcony station. The westerly dominates though it is interesting that wind doesn't reach as high as 50 m s-1 like in South-Col. South-Col station is placed at the top of the ridge between Lhotse and Mt. Everest and thus the wind forcing due to the mountain topography result in high wind speed. The lower wind speed shown in Balcony could also be due to the abrupt termination of data in mid-December when the wind speed might have begun rising quickly as we know the maximum wind speed was reached at the beginning of 2020.

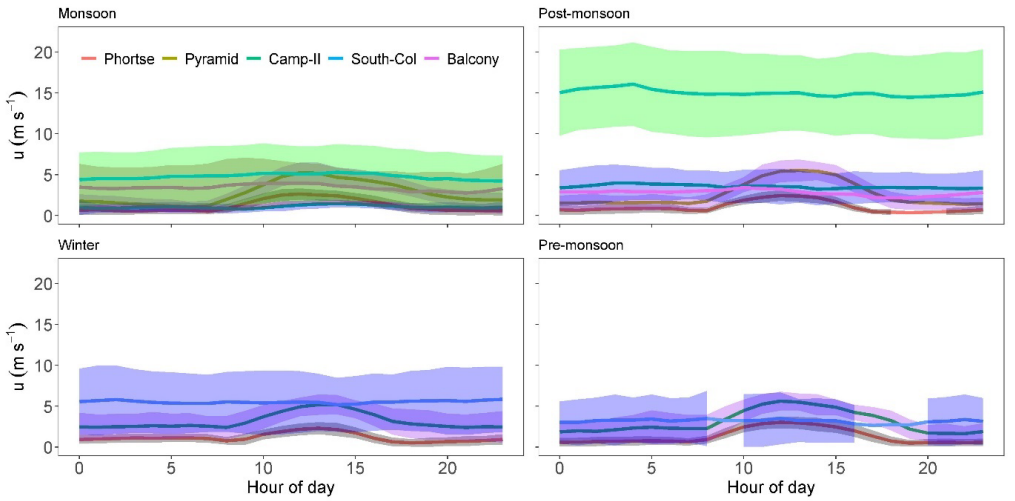

Figure 7. *Diurnal cycle of wind speed for Monsoon, Post-monsoon, Winter, and Pre-monsoon. Solid lines show the hourly mean and the shaded portion gives the plus-minus of standard deviation.*

At these stations, wind speed patterns are similar during the morning hour and evening hour. During the afternoon 12:00- 14:00 P.M. wind speed reaches maximum (Figure 7.) due to the variation in temperature difference between near-surface and ambient atmosphere. The region shows three kinds of wind patterns (i) wind speed increase from Phortse to Pyramid, (ii) after Pyramid station wind speed decrease and, (iii) high and uniform wind speed with strong wind gust mostly affected by the synoptic-scale pattern.

The lower station, Phortse, and Pyramid show the most variation due to the existence of anabatic (8:00 to 13:00) and katabatic wind (14:00 to 17:00). However, the

higher elevation station shows almost no variation. In post-monsoon, the higher wind speed seen in the South-Col station is driven more by regional wind circulation, plus the station lies at the pass between two ridges. The same is not seen for the Balcony because Mt. Everest acts as a barrier against the western wind. The same might have been seen in winter when the jet stream is at its strongest. In the lower station, the wind is mostly affected by the local circulation and underlying terrain, whereas wind is mostly affected by the synoptic-scale circulation in the higher stations.

Meteorological data observation and collection, AWS maintenance in the Nepalese Himalaya is always tough and continuous data for a long time in such elevation is tougher (Immerzeel et al., 2014; Shea et al., 2015). This is apparent for wind speed where the Young 05108-45 wind vane for South-Col and Balcony was damaged in winter due to high wind speed. However, the station itself was not damaged as we get the continuous radiation data, and thus, albedo, through which we can infer snow cover during winter.

4.1.5 Precipitation

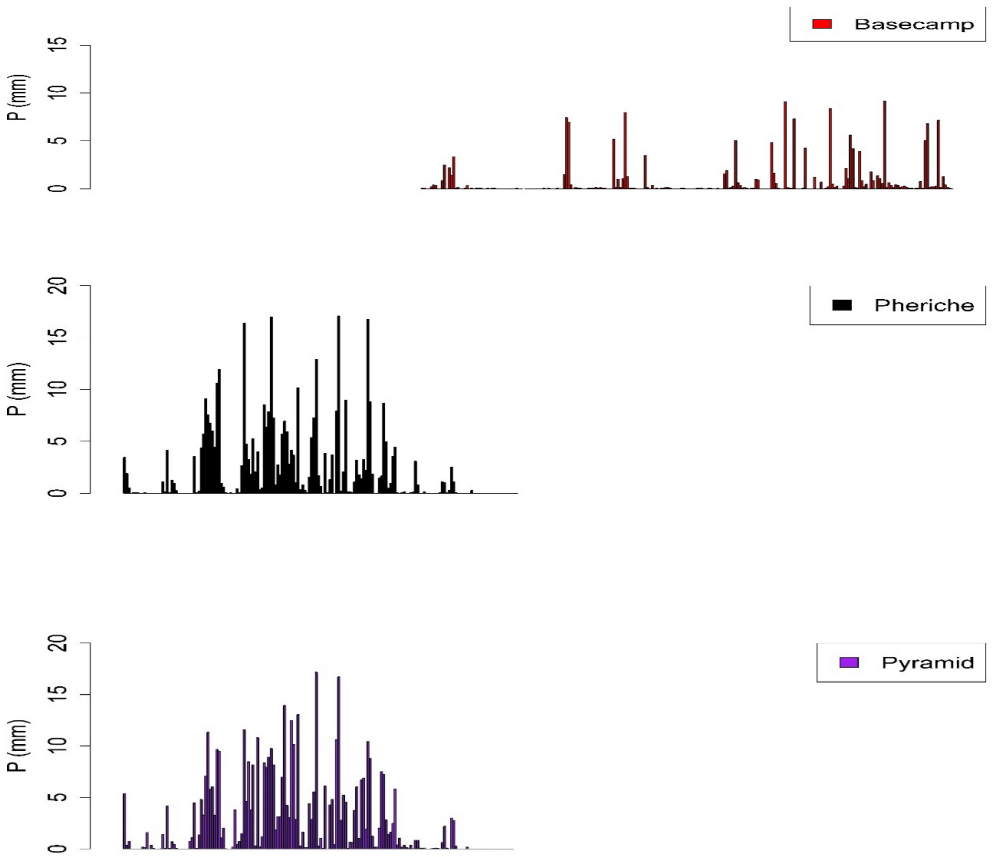

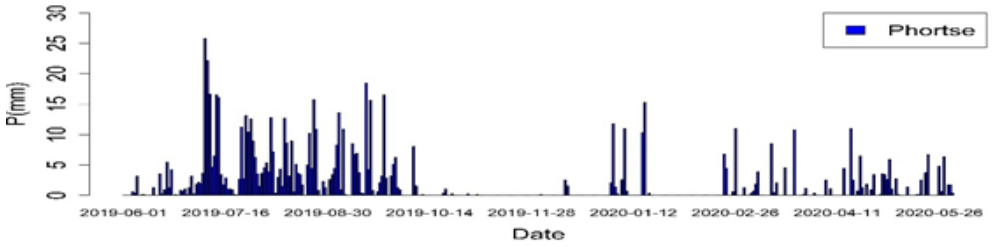

Figure 8. *Mean daily precipitation at Phortse, Pheriche, Pyramid, and Basecamp station. The gap is due to the station error during that period.*

The total mean daily precipitation are shown in Figure 8. Total mean daily precipitation highly varies in each station during every season. During the monsoon season, precipitation is high in every station. Phortse receives the highest daily precipitation of 530 mm during the monsoon season. Pheriche and pyramid receive about 364.03 mm and 430 mm, respectively (Table 2) which is greater than a previous finding of Bollasina et al. (2002) and Shea et al. (2015) at the pyramid site. It is noteworthy to mention that Pyramid receives more precipitation then Pheriche despite having the 665 m difference in elevation. Compared to Phortse station, precipitation in Pheriche decreased by 31% (166.34 mm) during monsoon. From Pheriche to Pyramid, the precipitation increased by 18% (66.34 mm). During the post-monsoon, mean daily precipitation at all stations receive less than 15 mm. Precipitation occur mainly in the form of snow in the winter season.

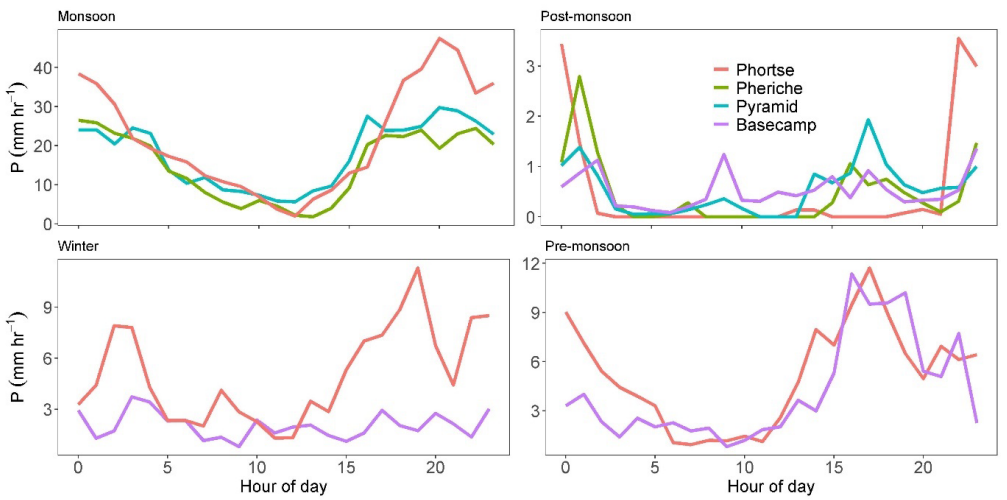

Figure 9. *Diurnal cycle of precipitation for Monsoon, Post-monsoon, Winter, and Pre-monsoon at different AWS sites.*

At high altitudes, the timing and magnitude of precipitation can have a significant impact on snow and ice melt, as the phase is determined by the air temperature. Diurnal precipitation is characterized by periodic maxima and minima. Monsoon has a gentle rise and dip of precipitation at the mid-range elevation. Sharp contrast exists in winter and Pre-monsoon, where Phortse has maximum precipitation during early morning and afternoon, while at Basecamp the maximum precipitation is observed in the late afternoon to evening in Pre-monsoon (Figure 9), partly owning to lag in heat-driven convective activities. The post-monsoon sees the most variation in diurnal precipitation among the stations but the overall pattern of early morning and late afternoon holds. In monsoon, high precipitation during nighttime is mainly due to the convergence between prevailing upslope flow with downwelling mountain breezes (Perry et al., 2020).

The precipitation amount in the Everest region increases with an elevation below 2500m a. s. l. but decreases with an elevation beyond 2500m a. s. l. (Salerno et al., 2015). The figure shows the seasonal variations in mean precipitation along the valley. The precipitation amount at Phortse (3810m a. s. l.) is higher than other stations. The precipitation decreases from the Phortse to the Pheriche and slightly change above the Pheriche station in the monsoon season which is similar to the previous finding by Yang et al., (2018) and Perry et al., (2020). The mean daily precipitation at Phortse station is 4.3 mm/day and at Pheriche station precipitation drop to 2.95mm/day and slightly increases.At the Pyramid station with mean daily precipitation 3.49 mm/day during the monsoon season. From post-monsoon total precipitation decrease at high elevation and most of it falls as snow (Salerno et al., 2015; Yang et al., 2018).

Season/ Station	Monsoon	Post-monsoon	Winter	Pre-monsoon	Annual
Phortse	530	12	120	123	785
Pheriche	364	11	-	-	-
Pyramid	430	13	-	-	-
Basecamp	-	12	49	100	-

Table 2. Total seasonal and annual precipitation (mm) at different AWS sites. Annual precipitation at Pheriche, Pyramid, and Basecamp stations was not calculated due to the missing data.

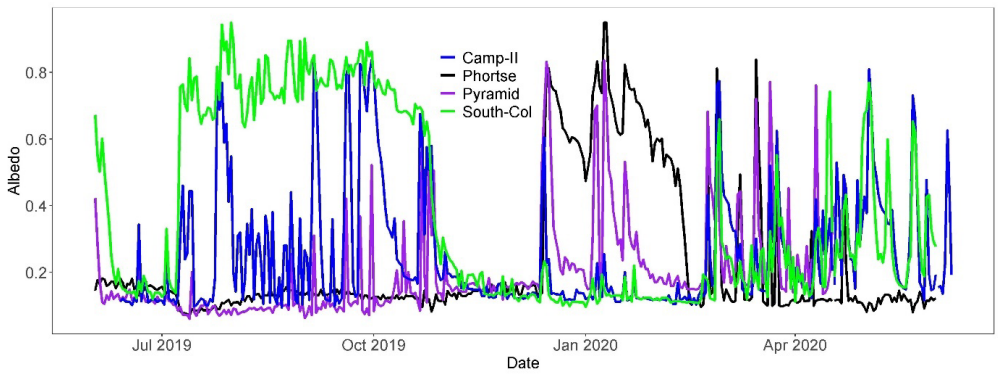

Figure 10. Mean daily albedo of the meteorological year 2019-2020, at different AWS.

At high-altitude above 4500 m a. s. l., albedo calculated from the incoming and outgoing shortwave radiation gives information about the form of precipitation and the duration of snow cover in different seasons. Albedo plays a critical role on the glacier surface through surface-atmosphere energy exchange, the variability of which influences glacier mass balance as well as water resources. The mean daily albedo shows, in the glacierized region the albedo increases as the increase of elevation during the monsoon season and terrain shield influence the spatial distribution of snow cover area (Wang et al., 2015). The albedo in upper and lower stations are opposite, one having maximum in monsoon and the other having maximum in winter respectively, and vice-versa for minimum. Figure 11 points out 0o isotherm being above 5000 meter with a degree of variation in monsoon. In effect, precipitation above these elevation falls as snow and lower temperature means the snowpack persists with relatively high albedo as seen in Figure 10 for South-Col and Camp-II. For lower elevation, higher temperature and rainfall much of the time ensures snow melt and hence, lower albedo. In winter, however, higher stations sees a high wind speed (Figure 6), especially westerlies that blows away the snow, resulting in ground exposure. Similarly, the wind speed is not strong enough to dissipate the snow and temperature below freezing ensures the persistence of snow and thus a high albedo for Pyramid and Phortse stations(Matthews et al., 2020; Shea et al., 2015).

4.2 Variation in temperature gradient (TG) and zero-degree isotherm

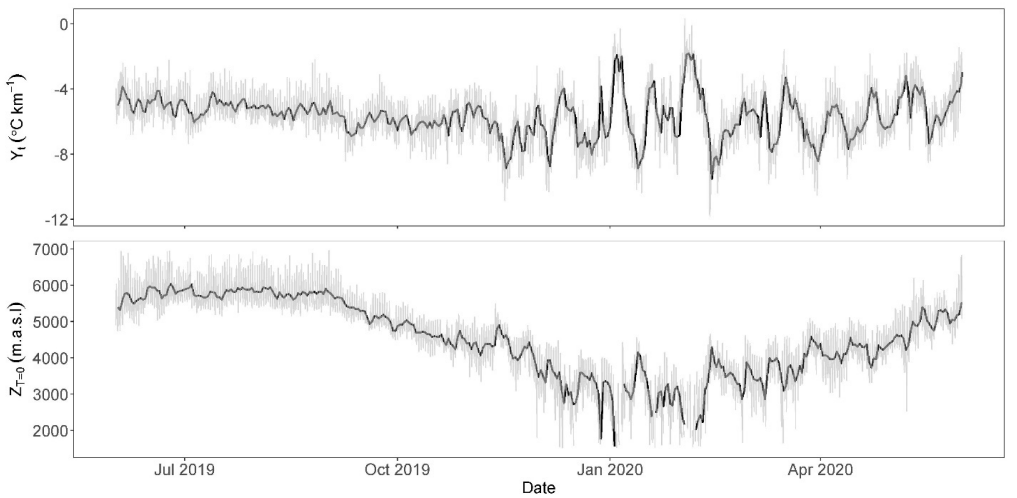

Figure 11. *Temperature gradient (top) and zero-degree isotherm (bottom) at the Khumbu catchment. Hourly value in grey and mean daily value in black.*

Temperature gradient computed from hourly observed data at Phortse and Camp-II station highlights the importance of weather stations on higher elevations. At daily periods, temperature gradients vary from -4 to -7 ℃ km-1 during winter and post-monsoon. This is less negative during the monsoon period (-4 to -5 ℃ km-1). During study period, the lowest temperature gradient is -9.5 ℃ km-1 as shown in Figure 11. This

is consistent with the previous study done in the Mera region, other parts of the Koshi basin (Mera Peak region), using four year data from 2013-2016 (Khadka et al., 2019). Immerzeel et al. (2014) and Shea et al. (2015) have also reported similar observation from the transect of Langtang Valley, Central Nepal. Compared with monsoon and post-monsoon, high variation is observed during winter and through pre-monsoon. The calculated height of the estimated zero-degree isotherm varies from approximately 3000 m a. s. l. in the winter to 6000 m a. s. l. during the monsoon. In this region, the Khumbu glacier is situated from 4700 to 7600 m a. s. l., which means glaciers in the region experienced melt and liquid precipitation during the monsoon.

At Phortse and Camp-II AWS station, calculated vapor pressure gradient range from 0 to -4 hPa km-1 throughout the year. The strong gradient during monsoon results in 6.11 hPa isoline values at approximately 6000 m a. s. l. and lower in the rest of the year as shown in the Figure 12.

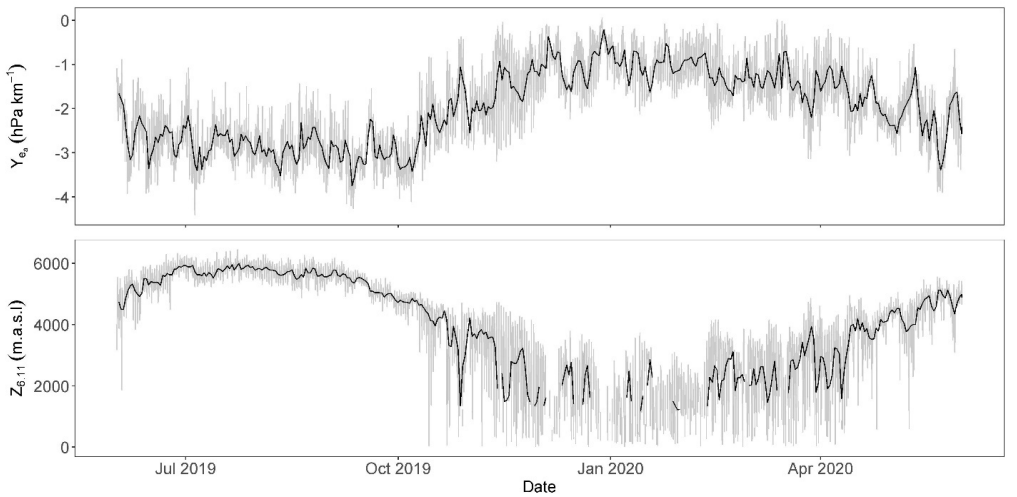

Figure 12. *Vapor pressure gradient (top) and 6.11 hPa isoline (bottom) at the Khumbu catchment, 2019-2020, hourly value in grey and mean daily value in black.*

The vapor pressure gradient (VPG) ranges from 0 to 3 hPa which is similar to Shea et al. (2015). During the monsoon, VPG remains high which leads to an increase in 6.11 hPa isoline near the 6000 m a. s. l., but in other seasons VPG remains lower. This means glaciers in the Khumbu region experience sublimation from the surface as well as snow line also moves higher elevation, which is important for the surface energy balance for the glacier. The zero-degree isotherm and 6.11hPa isoline during the monsoon season lie near the 6000 m a. s. l. and during another season the altitudinal line remains lower than 5000 m a. s. l.

Diurnal Cycle of Temperature and Vapor pressure gradient

The mean diurnal cycle of temperature gradient (TG) was calculated from the two stations Phortse and Camp-II station from June 2019 to May 2020. The temperature gradient is found least negative between 7:00 to 8:00 A.M (Figure 11). The temperature

gradient in winter is lowest (-7℃ km-1) which may be due to low moisture content in atmosphere. During pre-monsoon and monsoon TG, this is higher than -6℃ km-1 for nighttime and lower during daytime.

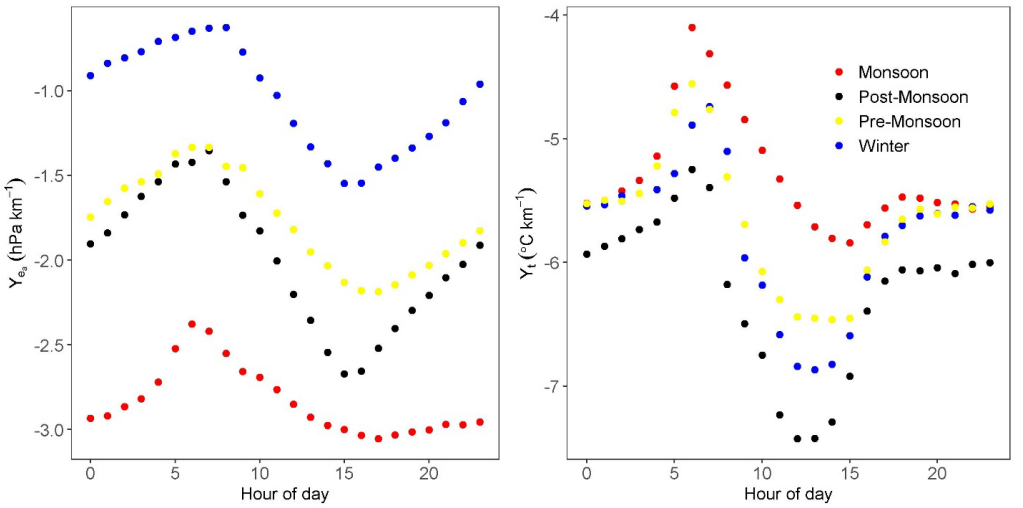

Figure 13. *Mean hourly vapor pressure gradient (left) and temperature gradient (right) for monsoon, Post-monsoon, Winter, and Pre-monsoon.*

The calculated diurnal cycle of vapor pressure is higher negative during the monsoon season (-2.5 to -3 hPa km-1) and least negative during the winter season (0 to -1.5 hPa km-1). In all seasons there is high VPG in early morning (6:00 to 7:00 A.M) and lower VPG in afternoon i.e., 3 P.M. In contrast, VPG reaches maximum after the late afternoon in monsoon (Figure 13).

4.3 Temperature Lapse Rate

In this study, increasingly negative Lapse Rate, compared with the seasonal value, are considered as the higher decrease of temperature with increasing elevation, and while the fewer negative values are considered as the temperature inversion. The increase in temperature from winter to monsoon is obvious throughout the valley. The temperature and elevation relationship is strong, and temperature can be predicted accurately as a function of elevation. During winter temperature interrupt in linearity is due to the coldest temperature and stable atmosphere.

Table 3. *Result of the regression between seasonal mean temperature and elevation, where, Cm maximum constant temperature at zero elevation, Lapse Rate is temperature lapse rate in ℃ km-1, r is correlation coefficient.*

Season	C_m	Lapse Rate (℃ km^{-1})	r
Monsoon	31.85	-5.6	0.99
Post-monsoon	32.74	-7	0.98
Winter	24.99	-6.8	0.97
Pre-monsoon	29.33	-6.7	0.97

During monsoon, the temperature reaches its highest and the lapse rate is less negative (-5.7 ℃ km-1) than in winter (-6.9 ℃ km-1) due to the reduction in radioactive cooling, as during monsoon the temperature decrease with elevation is attenuated by the presence of a consistent cloud cover. Post monsoon has a steeper lapse rate (-7 ℃ km-1) is due to the relatively small thermal forcing effect after the rainy summer. Whereas the pre-monsoon season shows a lapse rate (-6.7 ℃ km-1) which corresponds to the clear weather season and considerable sensible heat flux (dry convection). This is steeper than monsoon.

The regression lapse rate was calculated for all seasons. Correlation coefficients are very high for all seasons and vary between 0.97-0.99. The correlation between mean temperature and elevation is lowest during pre-monsoon and winter (0.97) and reach highest during monsoon (0.99). Very high correlation for temperature-elevation relationship indicate elevation as the main controlling factor on air temperature variability under high-temperature conditions, which occur mainly during the day.

The calculated temperature lapse rate is higher than ELR in post-monsoon (-7 ℃ km-1) and during winter (-6.8 ℃ km-1) and pre-monsoon (-6.7 ℃ km-1) and lower in monsoon (5 ℃ km-1). This is consistent with Kattel et al., (2013) during monsoon and pre-monsoon and similar with Yang et al., (2018) in Mt Everest. During another period, the calculated lapse rate is higher than the previous study Kattel et al., (2013); Yang et al., (2018) are due to the surface characteristics and the which also associated with surface energy balance.

4.4 Precipitation Gradient

Table 4. *Vertical precipitation gradient (PGV) and horizontal precipitation gradient (PGH) in mm m-1 at Khumbu region.2019-2020.*

Season	PGV	PGH
Monsoon	-0.063	-0.0086
Post-monsoon	0.00075	0.000046
Winter	-0.045	-0.0037
Pre-monsoon	-0.0147	-0.0012

Precipitation Gradient is calculated from Phortse to Basecamp AWS vertical, and it shows the negative pattern except for the post-monsoon season, during the monsoon and winter season vertical precipitation decrease by 63% m-1 and 45% m-1 in the region. Calculated longitudinal precipitation gradient is negative during the monsoon,

winter, and pre-monsoon, and positive during the post-monsoon season (Immerzeel et al., 2014; Seko, 1987)

The calculated precipitation gradient is negative during the monsoon, winter, and pre-monsoon season except for post-monsoon which differs from the Langtang region. This shows that the both existence of vertical and horizontal precipitation gradient and mainly precipitation occur in this region by the orographic convection. In this study, during the monsoon season, there is a reduction in monsoon precipitation by ~63% m-1 moving from Phortse to Basecamp station in this basin but the station-wise precipitation increases from Pheriche to Pyramid station.

5. Conclusion

This study presents the analysis of seasonal and daily meteorological variables from 7 different automatic weather stations from Everest region i.e., Phortse, Pheriche, Pyramid, Base camp, Camp-II, South-Col and Balcony for one hydrological year data (June 2019 to May 2020). These observed values can be used for snow and ice melt modeling and dynamical downscaling.

There are four detectable seasons over the year—monsoon with most precipitation and high temperature; post-monsoon with gradually decrease in temperature; winter with low temperature and snow as precipitation form and pre-monsoon with gradually increase in temperature and occasional precipitation. Precipitation measurements support previous observations of early-morning and late-evening precipitation maxima during the monsoon in Khumbu and there is a strong seasonal difference in the precipitation patterns and their controlling mechanisms.

However, maintaining the stations at such elevation is a challenge. Only radiation and temperature have complete one-year record. Single year data is not enough to get the full picture of the meteorology and its interaction between the variables. Long-term operation of these stations would require building more robust version of the available meteorological stations, able to withstand high wind speed. Local participation is necessary for maintenance. Further extension of this data will facilitate towards understanding glacier-climate interaction and impacts of climate in the regional water availability.

Acknowledgements

We gratefully acknowledge the University Grants commissions, Sanothimi, Bhaktpur, Nepal for providing thesis grant and faculty research grant to conduct this research. We also would like to express our sincere gratitude to the National Geographic, Institute of Research for Development (IRD) and Tribhuvan University for providing the data sets

References

Bollasina, M., Bertolani, L., & Tartari, G. (2002). Meteorological observations at high altitude in the Khumbu Valley, Nepal Himalayas, 1994-1999. Bulletin of Glaciological Research, 19, 1–12.

Cannon, F., Carvalho, L. M. V., Jones, C., Norris, J., Bookhagen, B., & Kiladis, G. N. (2017). Effects of topographic smoothing on the simulation of winter precipitation in High Mountain

Asia. Journal of Geophysical Research: Atmospheres, 122(3), 1456–1474. https://doi.org/10.1002/2016JD026038

Dawadi, B., Sharma, S., Hamal, K., Khadka, N., Dhital, Y. P., & Mahato, S. K. (2021). Does the High Elevation Climate along Mt. Everest can be Represented by Lower Elevation Stations? Journal of Institute of Science and Technology, 26(2), Article 2. https://doi.org/10.3126/jist.v26i2.41549

Fujita, K., & Sakai, A. (2000). Air temperature environment on the debris-covered area of Lirung Glacier, Langtang Valley, Nepal Himalayas. IAHS PUBLICATION, 83–88.

Grey, L., Johnson, A. V., Matthews, T., Perry, L. B., Elmore, A. C., Khadka, A., Shrestha, D., Tuladhar, S., Baidya, S. K., Aryal, D., & Gajurel, A. P. (2022). Mount Everest's photogenic weather during the post-monsoon. Weather, 77(5), 156–160. https://doi.org/10.1002/wea.4184

Immerzeel, W. W., Petersen, L., Ragettli, S., & Pellicciotti, F. (2014). The importance of observed gradients of air temperature and precipitation for modeling runoff from a glacierized watershed in the Nepalese Himalayas. Water Resources Research, 50(3), 2212–2226. https://doi.org/10.1002/2013WR014506

Immerzeel, W. W., Van Beek, L. P., & Bierkens, M. F. (2010). Climate change will affect the Asian water towers. Science, 328(5984), 1382–1385.

Kattel, D. B., Yao, T., Yang, K., Tian, L., Yang, G., & Joswiak, D. (2013). Temperature lapse rate in complex mountain terrain on the southern slope of the central Himalayas. Theoretical and Applied Climatology, 113(3–4), 671–682. https://doi.org/10.1007/s00704-012-0816-6

Khadka, A. (2019). Meteorological Analysis of high altitude Automatic Weather Station data from the Everest Region [Thesis, Department of Hydrology and Meteorology]. https://elibrary.tucl.edu.np/handle/123456789/8515

Khadka, A., Matthews, T., Perry, L. B., Koch, I., Wagnon, P., Shrestha, D., Sherpa, T. C., Aryal, D., Tait, A., Sherpa, T. G., Tuladhar, S., Baidya, S. K., Elvin, S., Elmore, A. C., Gajurel, A., & Mayewski, P. A. (2021). Weather on Mount Everest during the 2019 summer monsoon. Weather, 76(6), 205–207. https://doi.org/10.1002/wea.3931

Khadka, A., Wagnon, P., Brun, F., Shrestha, D., Lejeune, Y., & Arnaud, Y. (2022). Evaluation of ERA5-Land and HARv2 Reanalysis Data at High Elevation in the Upper Dudh Koshi Basin (Everest Region, Nepal). Journal of Applied Meteorology and Climatology, 61(8), 931–954. https://doi.org/10.1175/JAMC-D-21-0091.1

Khadka, D., Babel, M. S., Shrestha, S., & Tripathi, N. K. (2014). Climate change impact on glacier and snow melt and runoff in Tamakoshi basin in the Hindu Kush Himalayan (HKH) region. Journal of Hydrology, 511, 49–60. https://doi.org/10.1016/j.jhydrol.2014.01.005

Matthews, T., Perry, B., Khadka, A., Sherpa, T. G., Shrestha, D., Aryal, D., Tuldahar, S., Thapa, N., Pradhananga, N., Athans, P., Sherpa, D. Y., Guy, H., Seimon, A., Elmore, A., Li, K., & Alexiev, N. (2022). Weather Observations Reach the Summit of Mount Everest. Bulletin of the American Meteorological Society, 103(12), E2827–E2835. https://doi.org/10.1175/BAMS-D-22-0120.1

Matthews, T., Perry, L. B., Koch, I., Aryal, D., Khadka, A., Shrestha, D., Abernathy, K., Elmore, A. C., Seimon, A., Tait, A., Elvin, S., Tuladhar, S., Baidya, S. K., Potocki, M., Birkel, S. D., Kang, S., Sherpa, T. C., Gajurel, A., & Mayewski, P. A. (2020). Going to Extremes: Installing the World's Highest Weather Stations on Mount Everest. Bulletin of the American Meteorological Society, 101(11), E1870–E1890. https://doi.org/10.1175/BAMS-D-19-0198.1

Maussion, F., Scherer, D., Mölg, T., Collier, E., Curio, J., & Finkelnburg, R. (2014). Precipitation Seasonality and Variability over the Tibetan Plateau as Resolved by the High

Asia Reanalysis*. Journal of Climate, 27(5), 1910–1927. https://doi.org/10.1175/JCLI-D-13-00282.1

Ouyang, L., Yang, K., Lu, H., Chen, Y., Lazhu, Zhou, X., & Wang, Y. (2020). Ground-Based Observations Reveal Unique Valley Precipitation Patterns in the Central Himalaya. Journal of Geophysical Research: Atmospheres, 125(5). https://doi.org/10.1029/2019JD031502

Perry, L. B., Matthews, T., Guy, H., Koch, I., Khadka, A., Elmore, A. C., Shrestha, D., Tuladhar, S., Baidya, S. K., Maharjan, S., Wagnon, P., Aryal, D., Seimon, A., Gajurel, A., & Mayewski, P. A. (2020). Precipitation Characteristics and Moisture Source Regions on Mt. Everest in the Khumbu, Nepal. One Earth, 3(5), 594–607. https://doi.org/10.1016/j.oneear.2020.10.011

Perry, L. B., Yuter, S. E., Matthews, T., Wagnon, P., Khadka, A., Aryal, D., Shrestha, D., Tait, A., Miller, M. A., O'Neill, A., Rhodes, S. R., Koch, I., Sherpa, T. G., Tuladhar, S., Baidya, S. K., Elvin, S., Elmore, A. C., Gajurel, A., & Mayewski, P. A. (2021). Direct observations of a Mt Everest snowstorm from the world's highest surface-based radar observations. Weather, 76(2), 57–59. https://doi.org/10.1002/wea.3854

Pratap, B., Sharma, P., Patel, L., Singh, A. T., Gaddam, V. K., Oulkar, S., & Thamban, M. (2019). Reconciling High Glacier Surface Melting in Summer with Air Temperature in the Semi-Arid Zone of Western Himalaya. Water, 11(8), Article 8. https://doi.org/10.3390/w11081561

Rees, H. G., & Collins, D. N. (2006). Regional differences in response of flow in glacier-fed Himalayan rivers to climatic warming. Hydrological Processes, 20(10), 2157–2169. https://doi.org/10.1002/hyp.6209

Salerno, F., Guyennon, N., Thakuri, S., Viviano, G., Romano, E., Vuillermoz, E., Cristofanelli, P., Stocchi, P., Agrillo, G., Ma, Y., & Tartari, G. (2015). Weak precipitation, warm winters and springs impact glaciers of south slopes of Mt. Everest (central Himalaya) in the last 2 decades (1994–2013). The Cryosphere, 9(3), 1229–1247. https://doi.org/10.5194/tc-9-1229-2015

Seko, K. (1987). Seasonal variation of altitudinal dependence of precipitation in Langtang Valley, Nepal Himalayas. Bull. Glacier Res, 5, 41–47.

Shea, J. M., Wagnon, P., Immerzeel, W. W., Biron, R., Brun, F., & Pellicciotti, F. (2015). A comparative high-altitude meteorological analysis from three catchments in the Nepalese Himalaya. International Journal of Water Resources Development, 31(2), 174–200. https://doi.org/10.1080/07900627.2015.1020417

Sherpa, S. F., Wagnon, P., Brun, F., Berthier, E., Vincent, C., Lejeune, Y., Arnaud, Y., Kayastha, R. B., & Sinisalo, A. (2017). Contrasted surface mass balances of debris-free glaciers observed between the southern and the inner parts of the Everest region (2007–15). Journal of Glaciology, 63(240), 637–651. https://doi.org/10.1017/jog.2017.30

Shrestha, D., Singh, P., & Nakamura, K. (2012). Spatiotemporal variation of rainfall over the central Himalayan region revealed by TRMM Precipitation Radar: PRECIPITATION AND ALTITUDE. Journal of Geophysical Research: Atmospheres, 117(D22), n/a-n/a. https://doi.org/10.1029/2012JD018140

Wagnon, P., Brun, F., Khadka, A., Berthier, E., Shrestha, D., Vincent, C., Arnaud, Y., Six, D., Dehecq, A., Ménégoz, M., & Jomelli, V. (2021). Reanalysing the 2007–19 glaciological mass-balance series of Mera Glacier, Nepal, Central Himalaya, using geodetic mass balance. Journal of Glaciology, 67(261), 117–125. https://doi.org/10.1017/jog.2020.88

Wang, J., Cui, Y., He, X., Zhang, J., & Yan, S. (2015). Surface Albedo Variation and Its Influencing Factors over Dongkemadi Glacier, Central Tibetan Plateau. Advances in Meteorology, 2015, 1–10. https://doi.org/10.1155/2015/852098

Yang, K., Guyennon, N., Ouyang, L., Tian, L., Tartari, G., & Salerno, F. (2018). Impact of summer monsoon on the elevation-dependence of meteorological variables in the south of central Himalaya: METEOROLOGY IN CENTRAL HIMALAYA. International Journal of Climatology, 38(4), 1748–1759. https://doi.org/10.1002/joc.5293

Yang, K., He, J., Tang, W., Qin, J., & Cheng, C. C. K. (2010). On downward shortwave and longwave radiations over high altitude regions: Observation and modeling in the Tibetan Plateau. Agricultural and Forest Meteorology, 150(1), 38–46. https://doi.org/10.1016/j.agrformet.2009.08.004